



ORIGINAL ARTICLE

Biosynthesized CuO nano-platelets: Physical properties & enhanced thermal conductivity nanofluidics



B.T. Sone*, A. Diallo, X.G. Fuku, A. Gurib-Fakim, M. Maaza

UNESCO-UNISA Africa Chair in Nanosciences-Nanotechnology, College of Graduate Studies, University of South Africa, Muckleneuk Ridge, PO Box 392, Pretoria, South Africa
Nanosciences African Network (NANOAFNET), iThemba LABS-National Research Foundation, 1 Old Faure Road, Somerset West 7129, PO Box 722, Western Cape, South Africa

Received 1 March 2016; accepted 15 March 2017

Available online 22 March 2017

KEYWORDS

Copper (II) oxide;
Green synthesis;
Raman spectroscopy;
Photoluminescence;
Nanofluids;
Thermal conductivity

Abstract This contribution reports for the first time, room temperature biosynthesis of p-type CuO nanoparticles carried out using *Callistemon viminalis*' flower extracts as a chelating agent in a process that is entirely green. Room temperature X-ray diffraction, attenuated IR total reflection spectroscopy, X-ray photoelectron and Raman spectroscopy investigations confirmed the formation of single phase Tenorite bcc monoclinic CuO nanocrystals post annealing in air, at 500 °C. Photoluminescence spectroscopy with UV emissions at 356 nm (3.47 eV) and broad visible emissions at 418 nm, 561 nm, and 664 nm, support the formation in air, at 200 °C, of CuO nanoparticles with high surface-to-volume ratios and defects. As a direct application, the biosynthesized CuO nanoplatelet-containing powder dispersed in de-ionized water showed an enhancement of the thermal conductivity from 6% to 34% and a significant stability of the PVP stabilized CuO-water nanofluid.

© 2017 The Authors. Production and hosting by Elsevier B.V. on behalf of King Saud University. This is an open access article under the CC BY-NC-ND license (<http://creativecommons.org/licenses/by-nc-nd/4.0/>).

* Corresponding author at: UNESCO-UNISA Africa Chair in Nanosciences-Nanotechnology, College of Graduate Studies, University of South Africa, Muckleneuk Ridge, PO Box 392, Pretoria, South Africa.

E-mail addresses: sonebert@tlabs.ac.za, sonebert@gmail.com (B.T. Sone).

Peer review under responsibility of King Saud University.



Production and hosting by Elsevier

1. Introduction

CuO is a p-type semiconductor with a direct narrow bulk band gap of 1.2 eV and a refractive index of 2.63. It crystallizes in the monoclinic phase with space group C2/c (No. 15). CuO has been shown to be applicable to gas sensors (Zhang et al., 2014; Gou et al., 2008), biosensors (Sun et al., 2013; Lu et al., 2014), high temperature superconductors (Yang et al., 2006), magnetic storage media (Zoolfakar et al., 2014), catalysis (Huang et al., 2012), water purification by photocatalysis (Yu et al., 2015), energy storage in supercapacitors (Dubal et al., 2013), batteries (Wang et al., 2010) and anti-fungal/anti-microbial agents (Raja Naika et al., 2015) in the agriculture and health sectors.

A wide variety of CuO nano-/microstructures have reportedly been prepared in the literature amongst which are nanoribbons (Liu and Zeng, 2004), nanorods (Yang et al., 2013), nanowhiskers (Mukherjee et al., 2011), core-shell and hollow structures (Deng et al., 2011), hierarchical flower-like (Chu et al., 2013), nanorods (Toboosung and Singjai, 2011), urchin-like structures (Xu et al., 2009), hollow nano-/micro-architectures (Li et al., 2010), dumb-bell (Wang et al., 2009), leaf-like nanoplates (Xiang et al., 2010) and nanoparticles (Bakhtiari and Darezereshki, 2011). For the synthesis of such a wide variety of CuO nano-/microstructures, numerous physical and chemical-based techniques have been adopted amongst which are high temperature thermal oxidation of Cu substrates in air or controlled oxygen atmospheres (Zhang et al., 2014); microwave-assisted synthesis of solutions containing ionic liquids and Cu(II) salts (Deng et al., 2011; Wang et al., 2006); hydrothermal synthesis using Cu(II)-containing precursor solutions (Wang et al., 2012); sonochemical synthesis (Yang et al., 2014); thermal decomposition of Cu(II) precursor solutions (Salavati-Niasari and Davar, 2009); solution synthesis using Cu(II) precursor solutions at 60 °C (Yang et al., 2013); electrochemical etching of Cu substrates and subsequent heat treatment at 180 °C (Fan et al., 2003) as well as precipitation-pyrolysis of Cu-based precursor solutions (Fan et al., 2003).

With a host of these methods the use of environmentally non-benign chemicals such as NaBH₄, NaOH, organic solvents such as dimethyl formamide, ionic liquids and surfactants is needed. To eliminate or mitigate the problem of adding to the environmentally toxic and hazardous trail these methods leave, greener methods of synthesis are being researched. One such promising method for environmentally friendly synthesis of metal oxide nanoparticles is bio-reduction/oxidation of metal precursor salts using plant-based extracts. This biosynthesis method makes possible cleaner synthesis of better stabilized metal/metal oxide nanoparticles in a manner that is facile and cost-effective (Salavati-Niasari and Davar, 2009).

While significant work has been reported on the use of plant-based extracts to prepare various metal/metal oxide nanoparticles, not much is reported on the use of these extracts for the green synthesis of CuO nanoparticles. Of these Sharma et al. (2015) report the synthesis of CuO nanoparticles from the leaf extracts of the plant *Calotropis gigantea*. Raja Naika et al. (2015) report the synthesis of CuO nanoparticles using aqueous extracts from leaves of the plant *Gloriosa superba* while Abboud et al. (2014) report the use of extracts of the marine algae *Bifurcaria bifurcata* on the biosynthesis of CuO nanoparticles (Abboud et al., 2014). Elsewhere, Thekkae Padil and Černík (2013) report the use of gum karaya, a natural non-toxic hydrocolloid for the synthesis of CuO nanoparticles. Other reports include the use of *Aloe vera*, *Tinospora cordifolia* and *Musa balbisiana* plant extracts for CuO nano-/microstructure synthesis (Patel and Bhattacharya, 2013; Udayabhanu et al., 2015; Tamuly et al., 2014). Based on this survey it is clear that green synthesis of CuO nanoparticles using plant extracts of *Callistemon viminalis* has not been reported in the literature.

We report for the first time therefore, the use of aqueous extracts of the red flowers of *Callistemon viminalis* as an effective agent for facile and rapid biosynthesis of CuO nanoparticles.

The relative advantage of *Callistemon viminalis* to other natural extracts lies not only in its occurrence at room temperatures, the rapidity of the synthesis (occurring under ~2 h), but also the observed shape anisotropy of some of the CuO nanoparticles – specifically nanoplatelets. Consequently this contribution highlights the use of aqueous extracts from red flowers of *Callistemon viminalis* for rapid biosynthesis of CuO nano-platelets and their application for enhanced thermal conductivity in CuO-water nanofluids.

2. Materials and methods

2.1. Biosynthesis process via *Callistemon viminalis*' aqueous extracts

Callistemon viminalis commonly known as bottle brush in view of its red flowers shaped in the form of traditional bottle brushes is a plant originally from Australia. Several studies showed that the red-dye extract obtained from the red *Callistemon viminalis* flowers is rich in flavonoids, saponins, steroids, alkaloids and triterpenoids (Salem et al., 2013). A summary of the isolated active compounds is reported in Table 1. The acid compounds such as the Betulic or the Oleanolic acids can act as bioactive agents in reducing metal-ion based precursors.

For the synthesis, fresh red flowers of *Callistemon viminalis* were collected from the Western Cape site of iThemba LABS, South Africa. 6.65 g of the cleaned red parts of the bottle-brush shaped flowers was heated in 250 ml of de-ionized water between 75 and 85 °C for 2.5 h yielding a red coloured extract of pH ~3.5. Upon cooling, the filtered red aqueous extract was added to 2.8 g of CuSO₄·5H₂O (Sigma–Aldrich, 97%). At room temperature, while swirling the Cu salt was observed, within 5 min, to dissolve completely in the red aqueous extract forming a greyish brown suspension. The resultant suspension was allowed to settle over a period of 1–2 h after which a green coloured supernatant over a brown/grey precipitate (presumably a mixture of CuO and Cu) was observed. The precipitate was separated from the aqueous solution, first by decanting and then by centrifuging at 3500 rpm 3 times over successive additions of de-ionized water. The final precipitate was dried at 200 °C (15 min) yielding a brown-coloured precipitate which when heated in air at 500 °C for 2 h gave rise to a brown-black/grey-black powder (presumably CuO). A schematic illustration of the biosynthesis process is seen in Fig. 1. In the following experimental sections, the focus will be on the sample annealed at 500 °C as it is at this threshold value that the formation of crystalline CuO could be confirmed. Annealing the powders at 500 °C in air would help to compensate for O deficiencies if any.

2.2. Structural, luminescent and thermal conductivity characterization techniques

Surface morphology of the prepared powders was carried out using an Auriga High Resolution Scanning Electron Microscope (HRSEM) coupled to an Oxford instruments X-Max solid state Silicon drift detector (20 keV) used for carrying out elemental analysis by Energy Dispersive X-ray Spectroscopy (EDS). High Resolution Transmission Electron Microscopy (HRTEM) was carried out in a TECNAI F2

Table 1 The active compounds contained in the natural red extract of the *Callistemon viminalis* flower.

Flavonoids:	-Pelargonidin-3,5-diglucoside(I), -Cyanidin-3,5-diglucoside (II), -Kampferol (III),
Monoterpenoids:	-β-pinene (IV) -1,8-cineol;
Tannins:	-Pyrogallol (V); -Catechol (VI);
Triterpenoids:	-Betulic acid (VII) -α-amyrin (VIII); -Oleanolic acid (IX) -B-sitosterol (X)

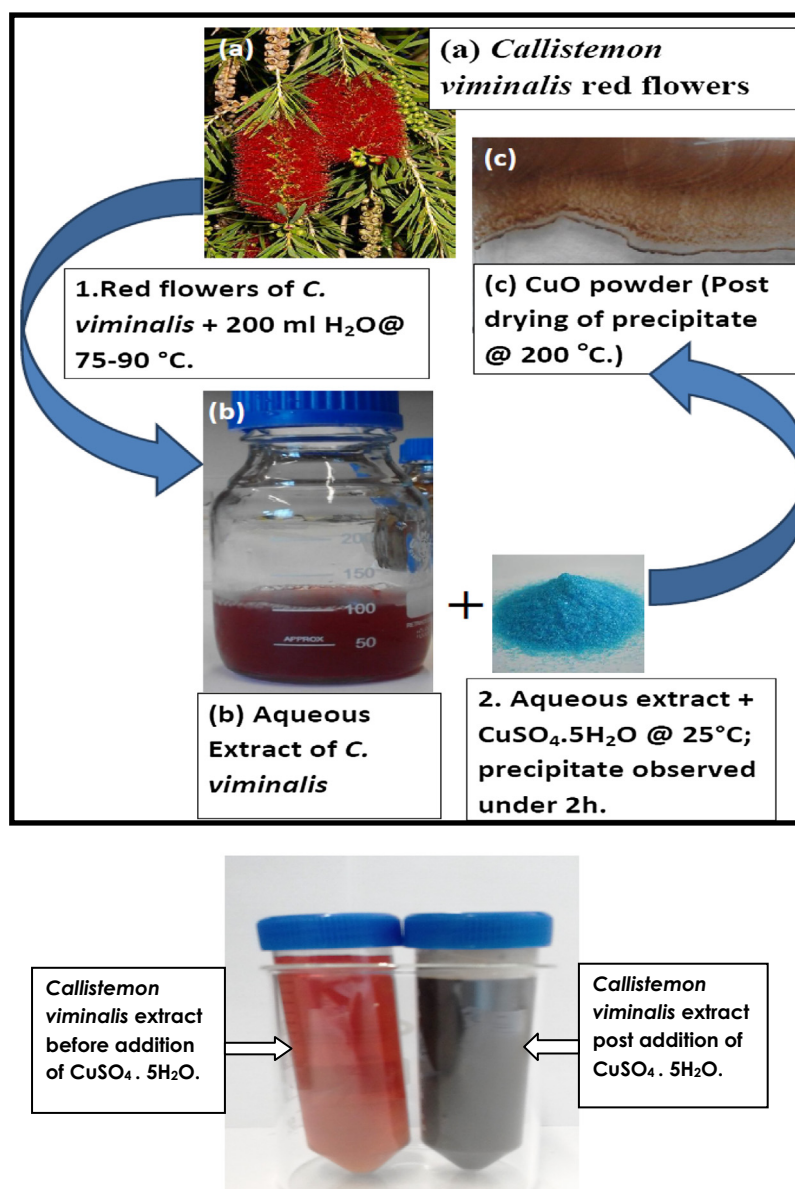


Figure 1 Schematic representation of the biosynthesis of CuO nanoparticles using aqueous extracts of *Callistemon viminalis*.

G20 HRTEM. The sample subjected to HRTEM was obtained by taking a swab of the thin film dissolved in ethanol using a Cu grid holder. Electron Dispersive X-ray Spectroscopy (EDS) was carried out using a specialized detector coupled to an OXFORD instruments nano-Scanning Electron Microscope. To determine the crystal structure of the prepared samples X-ray Diffraction (XRD) analysis was carried out using a Bruker Advanced D8 diffractometer with monochromated Cu K α radiation of 1.5406 Å operating in the Bragg–Brentano geometry. The zeta potential of the samples annealed at 500 °C was determined using the Malvern Zetasizer Nano ZS. Smoluchowski's model was used to calculate the zeta potential from measurements of the electrophoretic mobility.

To ascertain the presence of metal-oxo, metal-hydroxy bonds as well as detect the presence of other compounds surface bound to the expected CuO particles, Fourier-Transform Infrared spectroscopy was carried out in Attenu-

ated Total Reflection (ATR) mode with a diamond crystal employed for measurements. The Attenuated Total Reflection was obtained within a 400–4000 cm⁻¹ range using a Perkin Elmer 100 Spectrometer. For determining the vibrational modes in Cu–O based samples Raman spectroscopy was carried out using the 514.5 nm excitation line of an Ar⁺ laser source in the spectral range of 300–700 nm. X-ray Photoelectron Spectroscopy useful in determining the chemical states of Cu and O ions in the samples as well as ascertaining their purity was acquired using a constant 50 eV pass energy mode, in 0.1 eV increments at a 50 ms dwell time with the signal averaged for, at several regular scans. The XPS system was equipped with a dual Mg K α –Al K α anode for photoexcitation. The spectrum was calibrated with binding energy (BE) 284.5 eV for C1s electron.

Photoluminescence measurements were carried using a fibre-optics linked OCEANOPTICS system consisting of a

high-powered UV Light-emitting diode source (300 nm) coupled to a high sensitivity QE Pro-FL spectrometer that had a signal-noise ratio > 1000:1 and operated in a wavelength range of 185–1100 nm. Thermal conductivity of the CuO-water nanofluids was performed on a standard KD2 (Decagon Devices, Inc., USA). The measurements were performed at room temperature (25 °C) following initial tests on high quality ethylene glycol (Sigma–Aldrich) and de-ionized water for the calibration phase.

3. Results and discussions

3.1. Surface morphology, elemental analysis and growth mechanism

SEM-EDS results (Fig. 2) on the brown CuO powder were obtained from drying at ~200 °C, the brown precipitate ema-

nating from the CuSO₄-containing extract suggested the presence of agglomerated CuO, and possibly Cu nanoparticles were still held by some amount of glazed amorphous content. SEM analysis using Image J software gave the average particle size distribution (inset in Fig. 1) to be 14.9 ± 3.8 nm for about 71% of the measured particles and 42.4 ± 4.9 nm for the rest. Annealing of this brown CuO powder in air at 500 °C yielded a grey-black powder which under SEM revealed the formation of dense cuboids and hierarchical platelet-containing agglomerates. EDS confirmed the presence of Cu and Oxygen in the powders. The presence of C and S observed in the powder could be ascribed to the carbon film used to support the CuO samples as well as residual contributions from the CuSO₄ precursor and flower-based organic compounds that emanated from the aqueous extract.

Fig. 3 reports a Transmission Electron Microscopy (TEM) image while Fig. 4a reports Electron Dispersive X-ray Spec-

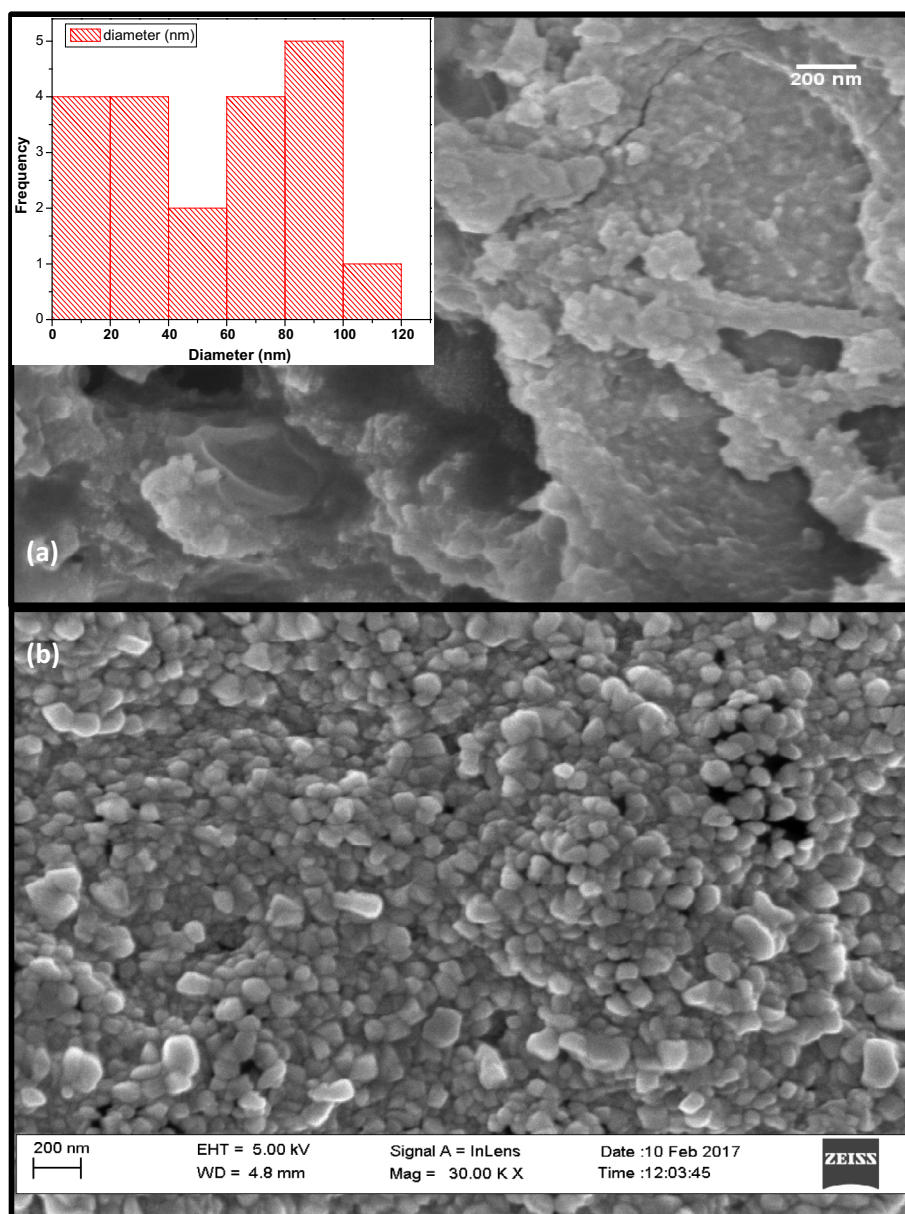


Figure 2 SEM micrograph for biosynthesized CuO nanoparticles annealed at (a) 200 °C for 2 h and (b) 500 °C, for 2 h.

troscopy (EDS) results of the brown CuO_x powder obtained from drying at $\sim 200^\circ\text{C}$ and heating in air at 500°C for ~ 2 h. The formed particles are highly agglomerated and nanoscaled within the size range from 19 to 200 nm as observed through Transmission Electron Microscopy (SEM). This effective agglomeration could be a severe disadvantage for potential technological applications. In this regard, a Zeta potential investigation was carried out after ultrasonication of the annealed CuO powders in water for 3–5 min. From this the zeta potential (Fig. 4b) was found to be 0.0758 ± 4.63 mV for CuO powder in water. This value shows that the CuO nanoparticles are of very low stability in water as was confirmed by their tendency to flocculate and sediment over time under 15 min, hence the need to further stabilize them using Polyvinylpyrrolidone. The tendency to aggregate/flocculate is due to strong attractive electrostatic forces that occur between the CuO nanoparticles.

3.2. Crystal structure elucidation using XRD analysis

The powdered samples of the as centrifuged precipitate, dried at 200°C and annealed at 500°C respectively were deposited onto float-glass substrates. The as-centrifuged and dried-at- 200°C samples both exhibited a semi-amorphous state while the annealed powder at 500°C displayed a crystalline structure (Fig. 5). The XRD spectrum (Fig. 5) observed presents 3 major Bragg peaks at $2\theta \sim 32.11^\circ$, $\sim 35.76^\circ$, and $\sim 38.96^\circ$ which are ascribed to reflections from the (-111) , (002) and (111) reticular planes respectively according to the JCPDS card 41-0254. Minor peaks include those at 48.86° , 53.35° , 58.39° , 61.93° , 66.96° and 67.99° which can be indexed to reflections from (-202) , (020) , (202) $(11-3)$, (-311) and (113) planes. Hence the crystallographic structure of the CuO_x nanocrystals is pure Tenorite CuO belonging to the bcc monoclinic Bravais lattice with space group $C2/c$ (C_{2h}^6) and unit cell lattice parameters $a = 4.65$, $b = 3.41$ and $c = 5.11$ where $a/b = 1.36$ and $c/b = 1.50 \pm 0.02$. The broadness of the Bragg peaks sustains

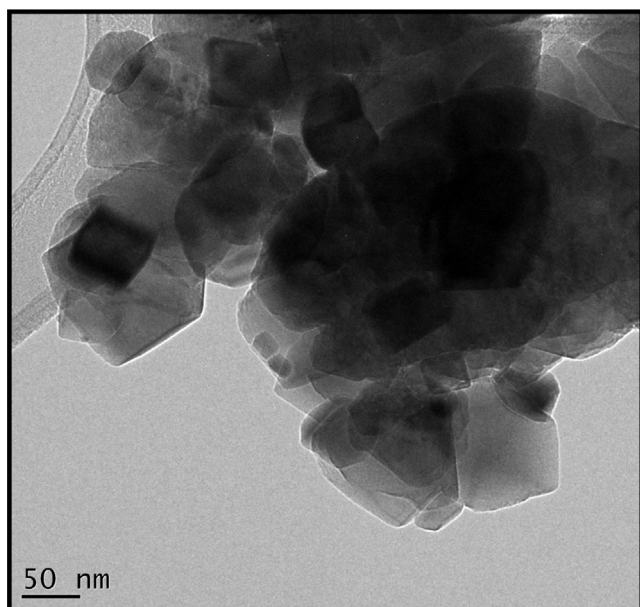


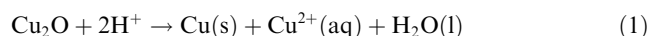
Figure 3 Transmission electron micrograph of the biosynthesized CuO powder annealed at 500°C in air, for 2 h.

the nanoscaled aspects of the Tenorite CuO crystallites. The crystallite size of the CuO nanoparticles could be estimated using the Debye–Scherrer approximation. The average size of the CuO nanocrystals is ~ 22 nm. It is worth mentioning that in addition to the broad peak observed between 20° and $35^\circ 2\theta$ emanating from the glass substrate, 2 other peaks observed at $\sim 25.74^\circ$ and $\sim 15.58^\circ$ may be attributed to the presence of carbon.

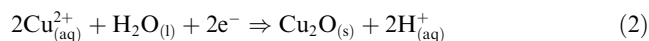
3.2.1. Growth mechanism

For a plausible mechanism of formation of CuO nanoparticles, considering that the aqueous extracts have a low pH of 3.5 we assume that the aqueous extract contains triterpenoid Betulinic and/or Oleanolic acids, two species reportedly present in *Calistemon viminalis*. The presence of these organic compounds gives the extract an acidic character which is determinant in the chemistry of the resultant solution and precipitate. Within the existing medium in which the biosynthesis occurs solvated Cu^{2+} ions could be reduced to Cu^+ or Cu^0 giving rise to the possible formation of $\text{Cu}(\text{OH})_2$, Cu_2O , CuO or Cu in the observed precipitate. We however rule out significant formation of $\text{Cu}(\text{OH})_2$ taking into consideration XRD analysis of the powders at 200°C as well as the absence of a blue colouration (colour of $\text{Cu}(\text{OH})_2$ in water) at any one time of the synthesis. That $\text{Cu}(\text{OH})_2$ does not form in the presence of surrounding water molecules may be explained as being a consequence of organic molecules preferentially binding with the Cu^{2+} ions in place of H_2O molecules.

Should there be formation of Cu_2O , the existing acidic medium ensures that any Cu_2O formed from the reduction of Cu^{2+} undergoes a disproportionation reaction to yield Cu^0 and Cu^{2+} ions (Eq. (1)) favouring therefore the formation of solid CuO and Cu nanoparticles.



Concurrent complexation of these Oleanolic and Betulinic acids (carboxylic acid-containing moieties) with Cu^{2+} ions arising from the dissolution of $\text{CuSO}_4 \cdot 5\text{H}_2\text{O}$, may give rise to Cu based metal-organic complexes which turn the previously red extract into a green-coloured supernatant post dissolution of the Cu salt. The green colour can be accounted for as resulting from the absorption, by the Cu-based complexes, of light in the red region of the visible spectrum. An additional role of the carboxylic acid-containing moieties as well as other organic molecules in the aqueous extract would be to help stabilize the CuO and Cu particles thereby limiting growth in an unidirectional manner for the as-synthesized particles – hence the fine nature of the particles even after drying in air at 200°C (SEM in Fig. 2a). Reduction of the Cu^{2+} ions to Cu^+ , and to a lesser extent Cu^0 , and their possible interaction with H_2O could result in the formation of brown Cu_2O leaving behind a supernatant richer in H^+ ions (Eq. (2)).



This scenario is supported by the fact that the pH of the supernatant post reduction of Cu^{2+} ions was observed to have dropped to ~ 1 . If formed, Cu_2O as already mentioned (Eq. (1)) is unstable in aqueous media and would undergo disproportionation to yield Cu and Cu^{2+} ions.

Again the formation of CuO and Cu is favoured and hence the brown colour of the precipitate collected. Should there be

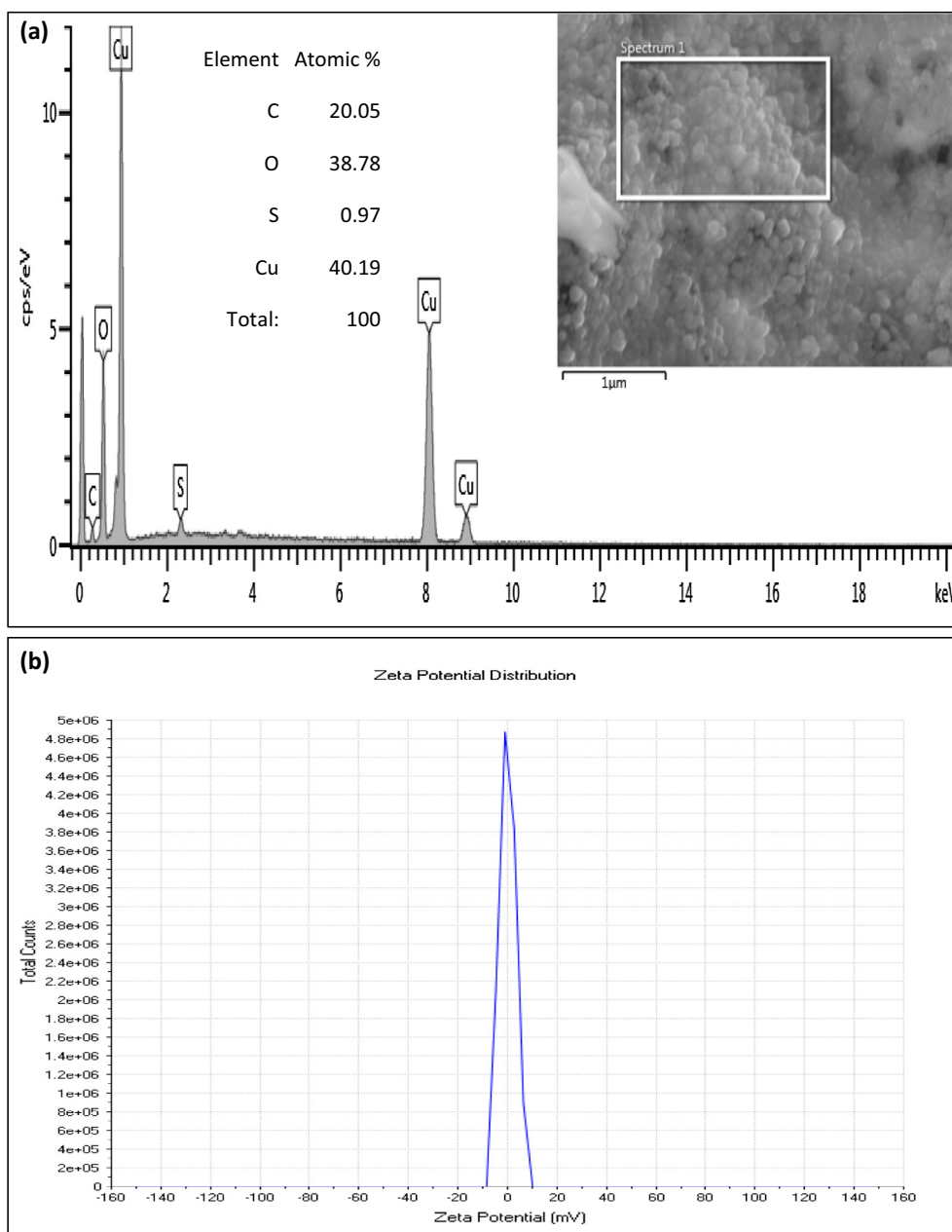


Figure 4 (a) Electron Dispersive X-ray Spectroscopy spectrum of biosynthesized nanoplatelet-containing CuO powder annealed at 500 °C, for 2 h. (b) Typical zeta potential measurement for biosynthesized CuO powder annealed at 500 °C, for 2 h.

Cu₂O and Cu within the brown precipitate upon synthesis, annealing in air between 25 and 200 °C temperatures both particle types will be simultaneously dehydrated and oxidized (Eqs. (3) and (4)) giving rise to an increase in the CuO nanoparticles.



Subsequent growth, rearrangement and coalescing of these CuO nanoparticles that occur during annealing from 200 to 500 °C give rise to an agglomeration of nanocubes and nanorods containing platelet-like structures.

3.3. Vibration spectroscopy investigations using FT-IR and Raman spectroscopy

To confirm the nature of the CuO Tenorite of the nanocrystals, both Attenuated Total Reflection-FT-IR (ATR-FTIR) and Raman spectroscopy investigations were conducted. Fig. 6 reports a typical ATR-FTIR spectrum of the brown CuO powder obtained from drying at ~200 °C and heated in air at 500 °C for ~2 h. The spectrum is split in 2 regions: the first and the second are lying between 400–800 cm⁻¹ and 2100–2700 cm⁻¹ respectively. The strong vibrational modes observed at 478.8, 529.3 and 578.6 cm⁻¹ are typical of Cu–O single bonds in the bending mode (Xu et al., 2010). The weak

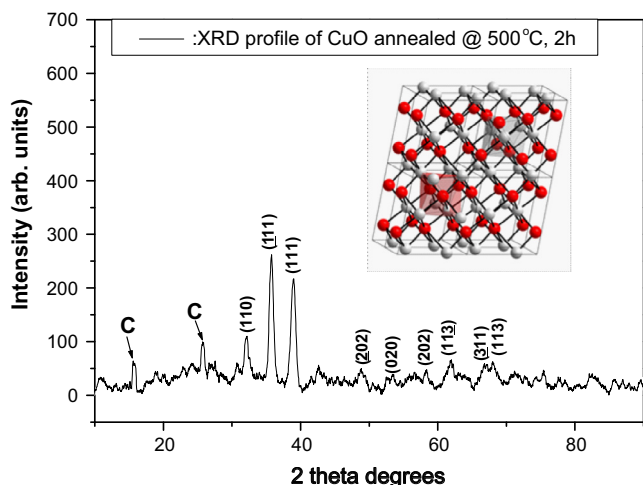


Figure 5 X-ray diffraction pattern of the CuO nanoplatelet-containing powder indicating the pure Tenorite structure.

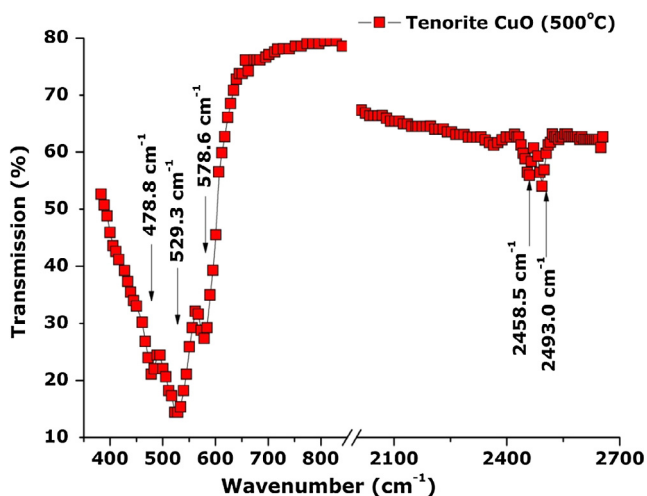


Figure 6 ATR/FT-IR spectrum of the CuO nanoplatelet-containing powder indicating the pure Tenorite structure.

bands observed at 2458.5 and 2493 cm^{-1} can be attributed to Cu—O bonds in the stretching mode. From the point of view of group theory the observed modes centred at 529 and 578.6 cm^{-1} are attributed to E_u and A_{2u} modes respectively. These 2 modes are characteristic of the pure Tenorite CuO phase (Xu et al., 2010). The absence of bands in the 1600 and 3300 cm^{-1} suggests the absence of waters of hydration/moisture within or at the surface of the CuO powders.

Based on XRD analysis, CuO prepared by this green synthesis is in the base-centred monoclinic phase. The Cu^{2+} ions are found at centres of inversion symmetry in a single fourfold site 4c (1/4, 1/4, 0), while oxygen ions occupy site 4e (0, y, 1/4) (Zhang et al., 2014). Monoclinic CuO from group analysis therefore has twelve zone-centre optical phonon modes with symmetries $4A_u + 5B_u + A_g + 2B_g$, of which only the A_g and $2B_g$ modes are Raman active (Zhang et al., 2014; Mukherjee et al., 2011; Xu et al., 1999; Reimann and Syassen, 1990). Raman peaks for monoclinic CuO crystal with a space group of $C2/c$ have thus been shown to be the A_g , B^1_g ,

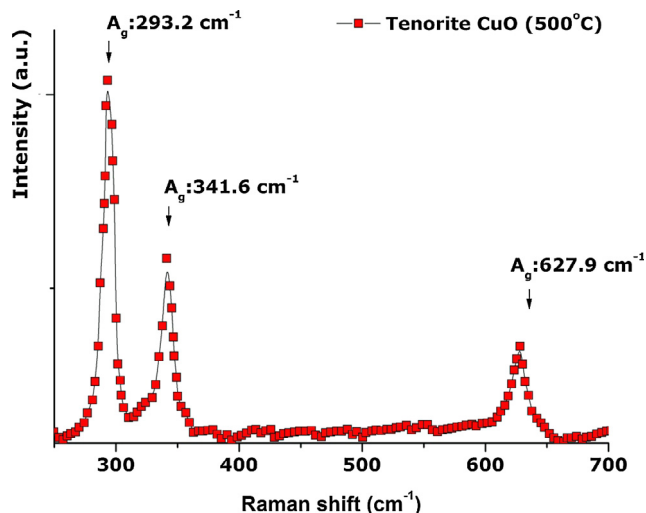


Figure 7 Room temperature Raman spectrum of the CuO nanostructured powder confirming the pure Tenorite structure.

and B^2_g phonon modes which appear at 303, 350, and 636 cm^{-1} , respectively (Chrzanowski and Irwin, 1989). All three phonon modes can be observed in the Raman spectrum of the annealed CuO nanoparticles (Fig. 7) we report. An intense peak at 293.2 cm^{-1} can be attributed to A^1_g vibrations while a shoulder peak at 341.6 cm^{-1} can be attributed to B^1_g vibrations. A broad peak of lower intensity at 627.9 cm^{-1} can be attributed to B^2_g phonon modes. These results, which are close to those reported by Chou et al. (2008) and Das et al. (2013), exhibit a slight red shift of ~ 9 cm^{-1} from bulk CuO. This red shift as well as the broad feature of all three peaks could be ascribed to a quantum confinement effect (Xu et al., 1999) or to strain/stress surface phenomena. The absence of Raman modes that can be attributed to Cu_2O suggests the CuO nanopowder is of high purity.

3.4. Chemical valence states via XPS studies

To confirm again the absence of Cu_2O phase and the purity of the Tenorite CuO nano-particles, X-ray Photoemission Spectroscopy (XPS) investigations (Fig. 8) were carried out. High resolution energy scans on the sample exhibited two main peaks at BE 933.5 and 953.5 eV corresponding respectively to Cu 2p_{3/2} and Cu 2p_{1/2} valence states of CuO (Krishnamoorthy and Kim, 2013). The splitting between these two states is about 20 eV. This is due to the formation of CuO nanostructures. The Cu 2p_{3/2} at 933.5 eV has a satellite peak with a doublet at 942 and 944 eV which is in agreement with the reported data (Krishnamoorthy and Kim, 2013). The BE at 539 eV corresponds to O1s of CuO and not Cu_2O and hence is in agreement with data reported by Krishnamoorthy and Kim (2013). The observed XPS profile strongly suggests the absence of Cu_2O , and also $\text{Cu}(\text{OH})_2$ impurities within the investigated sample.

3.5. Photoluminescence of CuO nanoparticles

The photoluminescent properties of the CuO nanoparticles dried in air at 200 °C for 10–12 h were investigated with the

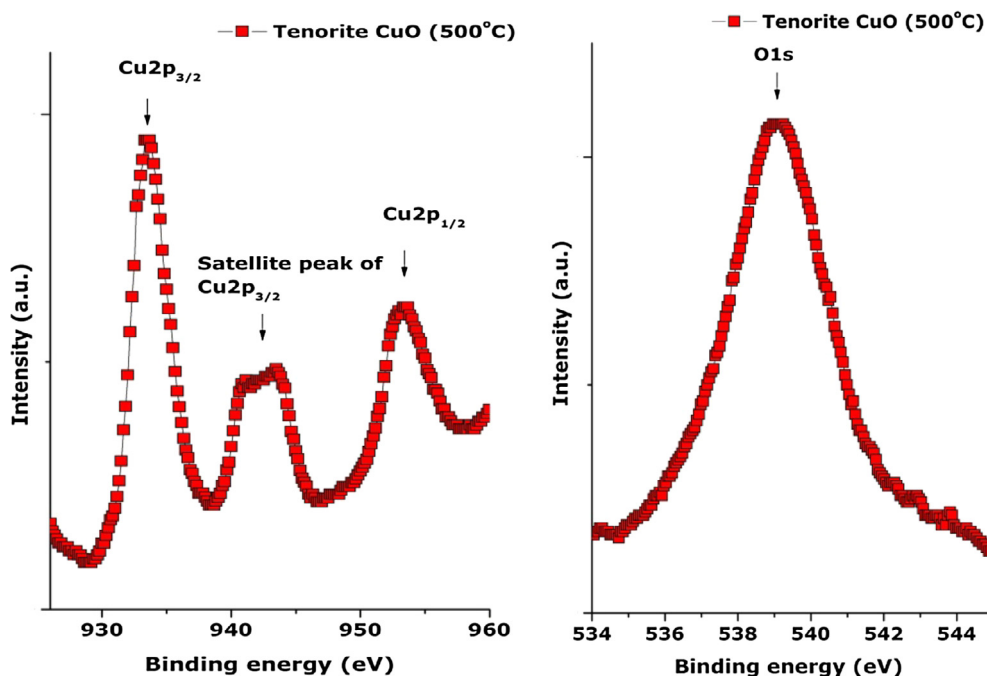


Figure 8 High-resolution XPS spectra of the CuO nanoplatelet-containing powder: (a) Cu 2p and (b) O1s.

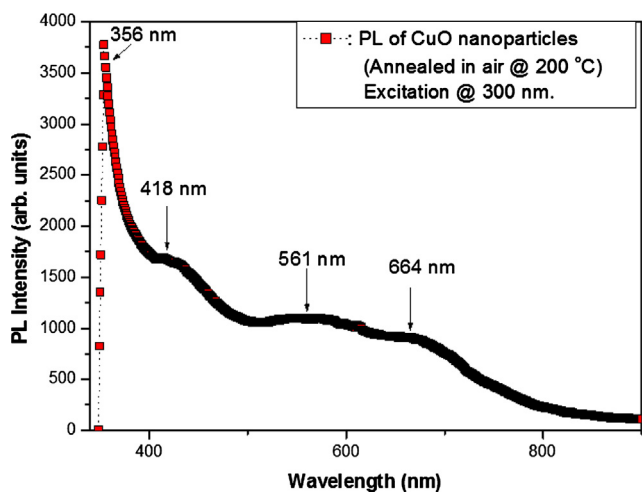


Figure 9 Photoluminescence spectrum of CuO nanoparticles annealed in air at 200 °C, with an excitation source of wavelength 300 nm.

aid of a fluorescence spectrometer by exciting with ultraviolet light of wavelength 300 nm. The resultant emission spectrum (Fig. 9) showed the occurrence of a strong UV emission peak at 356 nm which can be ascribed to band edge emissions that result from the recombination of electrons and holes of CuO free excitons (Dagher et al., 2014). When compared to bulk CuO UV-emission is blue shifted and can be ascribed to a quantum confinement effect which is a consequence of the presence of nanoplatelets in the CuO powders (Mohammed et al., 2014). A violet-blue luminescent band (shoulder peak) observed at ~418 nm is a typical near-band-edge emission peak of CuO (Sathyamoorthy and Mageshwari, 2013; Chang et al., 2005). The shoulder peak observed at 430 nm may be

ascribed to the existence of Cu vacancies in CuO which is a p-type semiconductor. The yellowish-green emission peak at 561 nm can be ascribed to deep level defects. These defects are said to occur only at low temperatures. The red emission peaks at 664 nm can be ascribed to multiple oxidation states of copper or the presence of singly ionized oxygen vacancies (Mohammed et al., 2014; Sathyamoorthy and Mageshwari, 2013). The broad nature of visible emissions encountered here in the violet-blue, yellowish-green and red regions of the visible spectrum suggests that CuO particles investigated here have a high surface-to-volume ratio with numerous surface-states and defects (vacancies and interstitials) which create trap levels responsible for the emissions observed (Mohammed et al., 2014; Huang et al., 2010).

3.6. CuO–H₂O nanofluids for enhanced thermal conductivity

One of the most prominent recent applications of nano-scaled CuO is within the nanofluid field (Farbod et al., 2015; Khodadadi et al., 2013). Indeed as indicated in Fig. 10, the thermal conductivity of CuO is amongst the highest of oxides approaching nearly 90 W/m K. Its use in the form of nano-dispersions in several fluids such as water, ethylene glycol, and mineral oil has clearly demonstrated a significant enhancement of the corresponding thermal conductivity. In this regard, several dispersions of the CuO nanoparticles in de-ionized water were prepared with volume fraction varying from 0.10% to 0.9%. To stabilize them, 15% by weight of Polyvinylpyrrolidone relative to the solid nanoparticle powder was added. Their initial dispersion was carried out in a 400 W ultrasonic power unit (UP400S, 400 W, 24 kHz) for ~2 h. Table 2 and Fig. 11 report the experimental values of k_{eff} versus the volume fraction at room temperature. As one can notice, there is a net increase in the effective thermal conductivity with the nanoplatelets' concentration. Yet, it is not a lin-

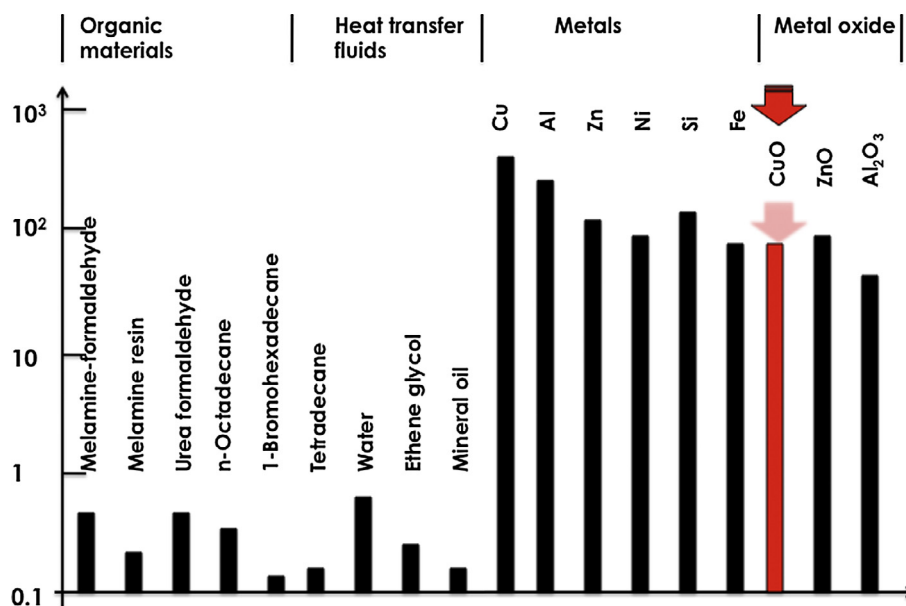


Figure 10 Thermal conductivity of various organic materials, heat transfer fluids, metals and oxides including CuO.

Table 2 Effective thermal conductivity and its enhancement at room temperature of various dispersions of CuO nanoplatelets in water, with polyvinyl pyrrolidone as a dispersing agent.

Volume concentration of CuO nanoplatelets (%)	Effective thermal conductivity k_{eff} (W/m K)	Average enhancement (%)
1	~0.623	05.83
1.5	~0.642	06.01
2	~0.661	11.10
3	~0.673	12.87
4	~0.679	15.29
5	~0.694	17.85
6	~0.734	18.86
6.5	~0.751	19.32
7.5	~0.778	32.38
8	~0.804	33.47
9	~0.817	34.00

ear relationship, and k_{eff} increases from ~0.623 to approximately ~0.817 W/m K. This corresponds to an enhancement from nearly 6% to 34%. These results are comparable to those of Khedkar et al. (2012) hence confirming the possibility of using the current green chemistry synthesized CuO nanoplatelets for enhanced thermofluid applications. It is necessary however, to mention that the CuO nanoparticles-water dispersions are stable up to 9% volume fraction. This could be due to the 2-D morphology of the CuO nanoplatelets present in these particles, and their surface/interface interaction with the polar H₂O molecules. The follow-up investigations would consist of studying their stability over time, their thermal cycling as well as duplicating the same approach with other nano-scaled oxides synthesized by a similar method (Sone et al., 2015; Thema et al., 2015; Thovhogi et al., 2015; Diallo et al., 2015a,b).

Also, for future work, as with previously synthesized nano-oxides prepared using *Callistemon viminalis*, *Agosthoma betulina*, *Aspalathus linearis* and *Hibiscus sabdarifa* natural extracts

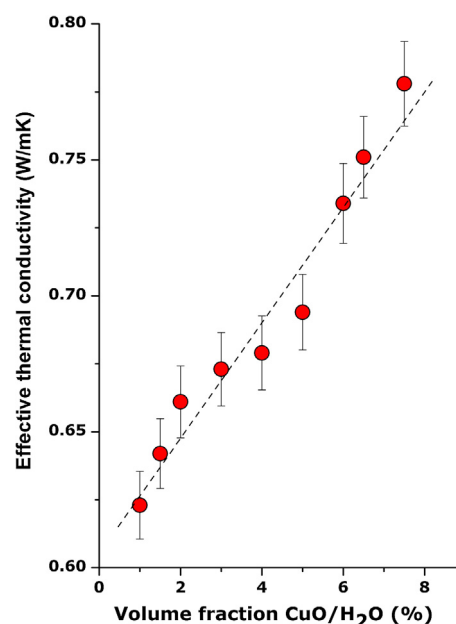


Figure 11 Room temperature evolution of the effective thermal conductivity of nanoplatelet-containing CuO powder dispersed in PVP-water solution versus their volume fraction.

(Sone et al., 2016; Thema et al., 2015; Thovhogi et al., 2015; Diallo et al., 2015a,b), it is necessary to use adequate techniques such as HPLC and GC-MS to identify the bioactive molecules present in the natural extracts as well as elucidate the reaction mechanisms that govern the interaction of the bioactive molecules with the precursor Cu salt.

4. Conclusion

Green synthesis of CuO Tenorite nanoparticles using a precursor CuSO₄ · 5H₂O salt was carried out at room temperature using aqueous extracts from red flowers of *Callistemon viminalis*. This rapid biosyn-

thesis that takes place under 1 h was observed to give rise to a brown coloured precipitate. Thermal annealing in air, for 2 h (at 500 °C), of the brown precipitate obtained after completely dissolution of the CuSO₄ pentahydrate salt in the aqueous extract resulted in the formation of nanoplatelet-containing grey-black CuO powders which stabilized in the base-centred monoclinic phase. XRD, ATR-FTIR, XPS, and Raman spectroscopy confirmed the nanocrystalline nature and the single phase aspect of the CuO nanoparticles. Blue shifts in the UV emission and broad visible emissions observed in the photoluminescence spectrum collected at $\lambda_{\text{excitation}} = 300$ nm, point to the existence of CuO nanoparticles with high surface-to-volume ratio and numerous defects. Dispersion of the CuO nanoparticles in PVP-stabilized water resulted in a significant enhancement from 6% to 34% of the thermal conductivity of the corresponding CuO-water nanofluid.

Acknowledgements

This research program was generously supported by grants from the National Research Foundation of South Africa (NRF), the French Centre National pour la Recherche Scientifique, iThemba LABS, the UNESCO-UNISA Africa Chair in Nanosciences & Nanotechnology, the Organization of Women in Science for the Developing World (OWSDW) and the Abdus Salam ICTP via the Nanosciences African Network (NANOAFNET) as well as the African Laser Centre (ALC) to whom we are grateful.

References

- Abboud, Y., Saffaj, T., Chagraoui, A., El Bouari, A., Brouzi, K., Tanane, O., Ihssane, B., 2014. Biosynthesis, characterization and antimicrobial activity of copper oxide nanoparticles (CONPs) produced using brown alga extract (*Bifurcaria bifurcata*). *Appl. Nanosci.* 4, 571–576.
- Bakhtiari, F., Darezereshki, E., 2011. One-step synthesis of tenorite (CuO) nano-particles from Cu₄(SO₄)(OH)₆ by direct thermal-decomposition method. *Mater. Lett.* 65, 171–174.
- Chang, S.-S., Lee, H.-J., Park, H.J., 2005. Photoluminescence properties of spark-processed CuO. *Ceram. Int.* 31, 411–415.
- Chou, M.H., Liu, S.B., Huang, C.Y., Wu, S.Y., Cheng, C.L., 2008. Confocal Raman spectroscopic mapping studies on a single CuO nanowire. *Appl. Surf. Sci.* 254, 7539.
- Chrzanowski, J., Irwin, J.C., 1989. Raman scattering from Cupric oxide. *Solid State Commun.* 70, 11–14.
- Chu, D., Mao, B., Wang, L., 2013. Microemulsion-based synthesis of hierarchical 3D flowerlike CuO nanostructures. *Mater. Lett.* 105, 151–154.
- Dagher, S., Haik, Y., Ayesh, A.I., Tit, N., 2014. Synthesis and optical properties of colloidal CuO nanoparticles. *J. Lumin.* 151, 149–154.
- Das, A., Venkataramana, B., Partheephan, D., Prasad, A.K., Dhara, S., Tyagi, A.K., 2013. Facile synthesis of nanostructured CuO for low temperature NO₂ sensing. *Phys. E (Amsterdam, Neth.)* 54, 40–44.
- Deng, C., Hu, H., Zhu, W., Han, C., Shao, G., 2011. Green and facile synthesis of hierarchical cocoon shaped CuO hollow architectures. *Mater. Lett.* 65, 575–578.
- Diallo, A., Beye, A.C., Doyle, T.B., Park, E., Maaza, M., 2015a. Green synthesis of Co₃O₄ nanoparticles via *Aspalathus linearis*: physical properties. *Green Chem. Lett. Rev.* 8, 30–36.
- Diallo, A., Ngom, B.D., Park, E., Maaza, M., 2015b. Green synthesis OF ZnO nanoparticles by *Aspalathus Linearis*: structural & optical properties. *J. Alloys Compd.* 646, 425–430.
- Dubal, D.P., Gund, G.S., Holze, R., Jadhav, H.S., Lokhande, C.D., Park, C., 2013. Surfactant-assisted morphological tuning of hierarchical CuO thin films for electrochemical supercapacitors. *Dalton Trans.* 42, 6459–6467.
- Fan, H., Yang, L., Hua, W., Wu, X., Wu, Z., Xie, S., Zou, B., 2003. Controlled synthesis of monodispersed CuO nanocrystals. *Nanotechnology* 15, 37–42.
- Farbod, M., Asl, R.K., Abadi, A.R.N., 2015. Morphology dependence of thermal and rheological properties of oil-based nanofluids of CuO nanostructures. *Colloids and surfaces A: physicochem. Eng. Aspects* 474, 71–75.
- Gou, X., Wang, G., Yang, J., Park, J., Wexler, D., 2008. Chemical synthesis, characterisation and gas sensing performance of copper oxide nanoribbons. *J. Mater. Chem.* 18, 965–969.
- Huang, C.-Y., Chatterjee, A., Liu, S.B., Wu, S.Y., Cheng, C.-L., 2010. Photoluminescence properties of a single tapered CuO nanowire. *Appl. Surf. Sci.* 256, 3688–3692.
- Huang, H., Zhang, L., Wu, K., Yu, Q., Chen, R., Yang, H., Peng, X., Ye, Z., 2012. Hetero-metal cation control of CuO nanostructures and their high catalytic performance for CO oxidation. *Nanoscale* 4, 7832–7841.
- Khedkar, R.S., Sonawane, S.S., Wasewar, K.L., 2012. Influence of CuO nanoparticles in enhancing the thermal conductivity of water and monoethylene glycol based nanofluids. *Int. Commun. Heat Mass Transfer* 39, 665–669.
- Krishnamoorthy, K., Kim, S.J., 2013. Growth, characterization and electrochemical properties of hierarchical CuO nanostructures for supercapacitor applications. *Mater. Res. Bull.* 48, 3136–3139.
- Khodadadi, J.M., Fan, L., Babaei, H., 2013. Thermal conductivity enhancement of nanostructure-based colloidal suspensions utilized as phase change materials for thermal energy storage: a review. *Renew. Sustain. Energy Rev.* 24, 418–444.
- Li, J.Y., Xiong, S., Pan, J., Qian, Y., 2010. Hydrothermal synthesis and electrochemical properties of urchin-like core-shell copper oxide nanostructures. *J. Phys. Chem. C* 114, 9645–9650.
- Liu, B., Zeng, H.C., 2004. Mesoscale organization of CuO nanoribbons formation of “dandelions”. *J. Am. Chem. Soc.* 126, 8124–8125.
- Lu, N., Shao, C., Li, X., Shen, T., Zhang, M., Miao, F., Zhang, P., Zhang, X., Wang, K., Zhang, Y., Liu, Y., 2014. CuO/Cu₂O nanofibers as electrode materials for non-enzymatic glucose sensors with improved sensitivity. *RSC Adv.* 4, 31056–31061.
- Mohammed, R.M., Harraz, F.A., Shawky, A., 2014. CuO nanobelts synthesized by a template-free hydrothermal approach with optical and magnetic characteristics. *Ceram. Int.* 40, 2127–2133.
- Mukherjee, N., Show, B., Maji, S.K., Madhu, U., Bhar, S.K., Mitra, B.C., Khan, Mondal, A., 2011. CuO nano-whiskers: electrodeposition, Raman analysis, photoluminescence study and photocatalytic activity. *Mater. Lett.* 65, 3248–3250.
- Patel, V.K., Bhattacharya, S., 2013. High-performance nanothermite composites based on aloe-vera-directed CuO nanorods. *ACS Appl. Mater. Interfaces* 5, 13364–13374.
- Raja Naika, H., Lingaraju, K., Manjunath, K., Kumar, D., Nagaraju, G., Suresh, D., Nagabhushana, H., 2015. Green synthesis of CuO nanoparticles using *Gloriosa superba* L. extract and their antibacterial activity, *Journal of Taibah University for Science* 9, 7–12.
- Reimann, K., Syassen, K., 1990. Pressure dependence of Raman modes in CuO. *Solid State Commun.* 76, 137–140.
- Salavati-Niasari, M., Davar, F., 2009. Synthesis of copper and copper (I) oxide nanoparticles by thermal decomposition of a new precursor. *Mater. Lett.* 63, 441–443.
- Salem, M.Z.M., Ali, H.M., El-Shanhorey, N.A., Abdel-Megeed, A., 2013. Evaluation of extracts and essential oil from *Callistemon viminalis* leaves: antibacterial and antioxidant activities, total phenolic and flavonoid contents. *Asian Pac. J. Trop. Med.* 6, 785–791.
- Sathyamoorthy, R., Mageshwari, K., 2013. Synthesis of hierarchical CuO microspheres: Photocatalytic and anti-bacterial activities. *Phys. E (Amsterdam, Neth.)* 47, 157–161.

- Sharma, J.K., Akhtar, M.S., Ameen, S., Srivastava, P., Singh, G., 2015. Green synthesis of CuO nanoparticles with leaf extract of *Calotropis gigantea* and its dye-sensitized solar cells applications. *J. Alloys Compd.* 632, 321–325.
- Sone, B.T., Manikandan, E., Gurib-Fakim, A., Maaza, M., 2015. Sm_2O_3 nanoparticles green synthesis via *Callistemon viminalis*' extract. *J. Alloys Compd.* 650, 357–362.
- Sone, B.T., Fuku, X.G., Maaza, M., 2016. Physical & electrochemical properties of green synthesized bunsenite NiO nanoparticles via *Callistemon viminalis*' extracts. *Int. J. Electrochem. Sci.* 11, 8204–8220.
- Sun, S., Zhang, X., Sun, Y., Yang, S., Song, X., Yang, Z., 2013. Hierarchical CuO nanoflowers: water-required synthesis and their application in a non-enzymatic glucose biosensor. *Phys. Chem. Chem. Phys.* 15, 10904–10913.
- Tamuly, C., Hazarika, M., Das, J., Bordoloi, M., Borah, D.J., Das, M. R., 2014. Bio-derived CuO nanoparticles for the photocatalytic treatment of dyes. *Mater. Lett.* 123, 202–205.
- Thekkak Padil, V.V., Černík, M., 2013. Green synthesis of copper oxide nanoparticles using gum karaya as a biotemplate and their antibacterial application. *Int. J. Nanomed* 8, 889–898.
- Thema, F.T., Beukes, P., Gurib-Fakim, A., Maaza, M., 2015. Green synthesis of Montepomite CdO nanoparticles by *Agathosma betulina* natural extract. *J. Alloys Compd.* 646, 1043–1048.
- Thovhogi, N., Diallo, A., Gurib-Fakim, A., Maaza, M., 2015. Nanoparticles green synthesis by *Hibiscus sabdariffa* flower extract: main physical properties. *J. Alloys Compd.* 647, 392–396.
- Toboosung, B., Singjai, P., 2011. Formation of CuO nanorods and their bundles by an electrochemical dissolution and deposition process. *J. Alloys Compd.* 509, 4132–4137.
- Udayabhanu, Nethravathi, P.C., Pavan Kumar, M.A., Suresh, D., Lingaraju, K., Rajanaika, H., Nagabhushana, H., Sharma, S.C., 2015. *Tinospora cordifolia* mediated facile green synthesis of cupric oxide nanoparticles and their photocatalytic, antioxidant and antibacterial properties. *Mater. Sci. Semicond. Process.* 33, 81–88.
- Wang, B., Wu, X., Shu, C., Guo, Y., Wang, C., 2010. Synthesis of CuO/graphene nanocomposite as a high-performance anode material for lithium-ion batteries. *J. Mater. Chem.* 20, 10661–10664.
- Wang, H., Shen, Q., Li, X., Liu, F., 2009. Fabrication of copper oxide dumbbell-like architectures via the hydrophobic interaction of adsorbed hydrocarbon chains. *Langmuir* 25, 3152–3158.
- Wang, T.X., Xu, S.H., Yang, F.X., 2012. Green synthesis of CuO nanoflakes from $\text{CuCO}_3 \cdot \text{Cu}(\text{OH})_2$ powder and H_2O_2 aqueous solution. *Powder Technol.* 228, 128–130.
- Wang, W., Zhu, Y., Cheng, G., Huang, Y., 2006. Microwave-assisted synthesis of cupric oxide nanosheets and nanowhiskers. *Mater. Lett.* 60, 609–612.
- Xiang, J.Y., Tu, J.P., Zhang, J., Zhong, J., Zhang, D., Cheng, J.P., 2010. Incorporation of MWCNTs into leaf-like CuO nanoplates for superior reversible Li-ion storage. *Electrochem. Commun.* 12, 1103–1107.
- Xu, J.F., Ji, W., Shen, Z.X., Tang, S.H., Ye, X.R., Jia, D.Z., Xin, X. Q., 1999. Raman spectra of CuO nanocrystals. *J. Raman Spectrosc.* 30, 413–417.
- Xu, L., Sithambaram, S., Zhang, Y., Chen, C.H., Jin, L., Joesten, R., Suib, S.L., 2009. Novel urchin-like CuO synthesized by a facile reflux method with efficient olefin epoxidation catalytic performance. *Chem. Mater.* 21, 1253–1259.
- Xu, Y., Wang, C., Chen, D., Jiao, X., 2010. Fabrication and characterization of novel nanostructured copper oxide films via a facile solution route. *Mater. Lett.* 64, 249–251.
- Yang, H., Liu, Q.Q., Li, F.Y., Jin, C.Q., Yu, R.C., 2006. Symmetry of unoccupied electronic states in the high-Tc superconductor $\text{Sr}_2\text{-CuO}_2 + \delta\text{Cl}_{2-y}$ studied by electron energy-loss spectroscopy. *Appl. Phys. Lett.* 88, 082502.
- Yang, X., Jiang, L., Mao, C., Niu, H., Song, J., Zhang, S., 2014. Sonochemical synthesis and nonlinear optical property of CuO hierarchical superstructures. *Mater. Lett.* 115, 121–124.
- Yang, Z., Wang, D., Li, F., Liu, D., Wang, P., Li, X., Yue, H., Peng, S., He, D., 2013. Facile synthesis of CuO nanorod for lithium storage application. *Mater. Lett.* 90, 4–7.
- Yu, J., Zhuang, S., Xu, X., Zhu, W., Feng, B., Hu, J., 2015. Photogenerated electron reservoir in hetero-p-n CuO-ZnO nanocomposite device for visible-light-driven photocatalytic reduction of aqueous Cr(VI). *J. Mater. Chem. A* 3, 1199–1207.
- Zhang, Q., Zhang, K., Xu, D., Yang, G., Huang, H., Nie, F., Li, C., Yang, S., 2014. CuO nanostructures: Synthesis, characterization, growth mechanisms, fundamental properties, and applications. *Prog. Mater. Sci.* 60, 208–337.
- Zoölfakar, A.S., Rani, R.A., Morfa, A.J., O'Mullane, A.P., Kalantar-zadeh, K., 2014. Nanostructured copper oxide semiconductors: a perspective on materials, synthesis methods and applications. *J. Mater. Chem. C* 2, 5247–5270.